J Comput Electron (2010) 9: 146–152
DOI 10.1007/s10825-010-0317-8

Stochastic modeling of bipolar resistive switching in metal-oxide based memory by Monte Carlo technique

Alexander Makarov · Viktor Sverdlov · Siegfried Selberherr

Published online: 7 October 2010

Abstract A stochastic model of the resistive switching mechanism in bipolar metal-oxide based resistive random access memory (RRAM) is presented. The distribution of electron occupation probabilities obtained is in agreement with previous work. In particular, a low occupation region is formed near the cathode. Our simulations of the temperature dependence of the electron occupation probability near the anode and the cathode demonstrate a high robustness of the low occupation region. This result indicates that a decrease of the switching time with increasing temperature cannot be explained only by reduced occupations of the vacancies in the low occupation region, but is related to an increase of the mobility of the oxide ions. A hysteresis cycle of RRAM switching simulated with the stochastic model including the ion dynamics is in good agreement with experimental results.

Keywords Resistive switching mechanism · Stochastic model · Monte Carlo method · RRAM

1 Introduction

The resistive switching phenomenon is observed in different types of insulators, such as metal oxides, perovskite oxides, and chalcogenide materials. Because the electrical conductance of the insulator can be set at different levels by the application of an electric field, this phenomenon becomes attractive for advanced memory concepts. Indeed, a state with high resistance can be interpreted as logical 1 and a state with low resistance as logical 0, or vice versa, depending on the technology. The concepts of memory using the resistive switching phenomenon can be conveniently divided into the following three categories: Conductive Bridge RAM (CBRAM), Phase Change RAM (PCRAM), and Resistive RAM (RRAM). CBRAM is based on a solid-state electrolyte in which mobile metal ions create a conductive bridge between the two electrodes under the influence of an electric field. PCRAM employs the difference in resistivity between the crystalline and amorphous phases of a chalcogenide compound. RRAM is based on metal oxides, such as TiO_x [1–4], HfO_2 [5], Cu_xO [6], NiO [7], ZnO [8], and perovskite oxides, such as doped $SrTiO_3$ [9], doped $SrZrO_3$ [10], $Pr_{1-x}Ca_xMnO_3$ [11], and employs the electric field induced difference in resistivity between the high and low current carrying states.

The increasing demand for miniaturization of microelectronic devices has significantly accelerated the search for new concepts of nonvolatile memory during the last few years. Memory based on charge storage (such as flash memory, and others) is gradually approaching the physical limits of scalability, and conceptually new types of memories based on a different storage principle are gaining momentum. Apart from good scalability, a new type of memory must also exhibit low operating voltages, low power consumption, high operation speed, long retention time, high endurance, and simple structure [12, 13].

In addition to RRAM, PCRAM, and CBRAM there exist several other concepts as potential replacements of the charge memory. Some of the technologies are already available in prototype form (such as carbon nanotube RAM

A. Makarov (✉) · V. Sverdlov · S. Selberherr
Institute for Microelectronics, Vienna University of Technology, Vienna, Austria
e-mail: makarov@iue.tuwien.ac.at

V. Sverdlov
e-mail: sverdlov@iue.tuwien.ac.at

S. Selberherr
e-mail: selberherr@iue.tuwien.ac.at

(NRAM)) [14], others as product (magnetoresistive RAM (MRAM) [15], ferroelectric RAM (FRAM) [16]), while the technologies of spin-torque transfer RAM (STTRAM) [17] and racetrack memory [18] are under intensive research.

From these concepts the CBRAM, PCRAM, and RRAM possess the simplest metal-insulator-metal (MIM) structure and, as a consequence, have good scalability. This fact gives advantages to RRAM, PCRAM, and CBRAM over other advanced memory concepts.

In addition to its simple structure RRAM is characterized by a low operating voltage (<2 V), fast switching time (<10 ns), high density, and long retention time.

Several physical mechanisms based on either electron or ion switching have been recently suggested in the literature: a model based on trapping of charge carriers [19], electrochemical migration of oxygen vacancies [20, 21], electrochemical migration of oxygen ions [22, 23], a unified physical model [24], a domain model [25], a filament anodization model [26], a thermal dissolution model [27], a two-variable resistor model [28], and others. Despite this, however, a proper fundamental understanding of the RRAM switching mechanism is still missing hindering further development of this type of memory.

We propose a stochastic model of the resistive switching mechanism based on electron hopping between the oxygen vacancies along the conductive filament in an oxide-layer, where a redox reaction plays a crucial role in the resistive switching from the state with low resistance to the state with high resistance and back.

2 Model description

We associate the resistive switching behavior in oxide-based memory with the formation and rupture of a conductive filament (CF). The CF is formed by localized oxygen vacancies (V_o) [24] or domains of V_o (Fig. 1). Formation and rupture of a CF is due to a redox reaction in the oxide layer under a voltage bias. The conduction is due to electron hopping between these V_o.

For modeling the formation and rupture of a CF in bipolar oxide-based memory by Monte Carlo techniques, we describe the dynamics of oxygen ions (O^{2-}) and electrons in an oxide layer as follows:

- formation of V_o by O^{2-} moving to an interstitial position;
- annihilation of V_o by moving O^{2-} to V_o;
- an electron hop into V_o from an electrode;
- an electron hop from V_o to an electrode;
- an electron hop between two V_o.

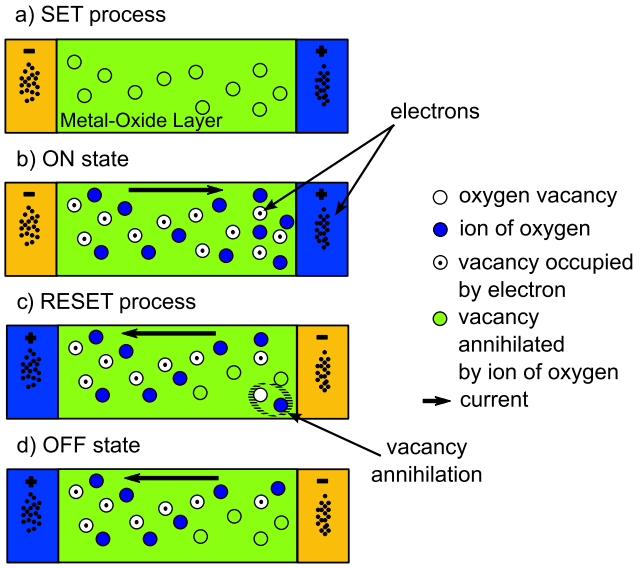

Fig. 1 Illustration of the resistive switching mechanism in a bipolar oxide-based memory cell: (**a**) Schematic illustration of the SET process. (**b**) Schematic view of the conducting filament in the low resistance state (ON state). (**c**) Schematic illustration of the RESET process. (**d**) Schematic view of the conducting filament in the high resistance state (OFF state). Only the oxygen vacancies and ions which impact the resistive switching are shown

In order to model the dependences of transport on the applied voltage and temperature we choose the hopping rates for electrons as [29]:

$$\Gamma_{nm} = A_e \cdot \frac{dE}{1 - \exp(-dE/T)} \cdot \exp(-R_{nm}/a) \tag{1}$$

Here, A_e is a coefficient, $dE = E_n - E_m$ is the difference between the energies of an electron positioned at sites n and m, R_{nm} is the hopping distance, a is the localization radius. The hopping rates between an electrode (0 or $N+1$) and an oxygen vacancy m are described:

$$\Gamma_m^{iC} = \alpha \cdot \Gamma_{0m}, \qquad \Gamma_m^{oC} = \alpha \cdot \Gamma_{m0} \tag{2}$$

$$\Gamma_m^{iA} = \beta \cdot \Gamma_{(N+1)m}, \qquad \Gamma_m^{oA} = \beta \cdot \Gamma_{m(N+1)} \tag{3}$$

Here, α and β are the coefficients of the boundary conditions on the cathode and anode, respectively, N is the number of sites, A and C stand for cathode and anode, and i and o for hopping on the site and out from the site, respectively.

To describe the motion of ions we have chosen the ion rates similar to (1):

$$\Gamma'_n = A_i \cdot \frac{dE}{1 - \exp(-dE/T)} \tag{4}$$

Here we assume that O^{2-} can only move to the nearest interstitial. A distance-dependent term is thus included in A_i. dE includes the formation energy for the m-th

V_o/annihilation energy of the m-th V_o, when O^{2-} is moving to an interstitial or back to V_o, respectively.

The current generated by hopping is calculated as:

$$I = q_e \cdot \sum dx \Big/ \sum \left(1 \Big/ \sum_m \Gamma_m \right) \tag{5}$$

3 Simulation tool

For modeling the RRAM switching behavior a simulation tool was developed which allows simulating 1D/2D/3D model systems. C++ was chosen as programming language. Figure 2 shows a flow chart of the simulation process performed by the tool. The module "starter" is a basic module which allows choosing different modes of simulation to produce results of a particular experiment of interest. The input parameters are set in an initialization file as shown below.

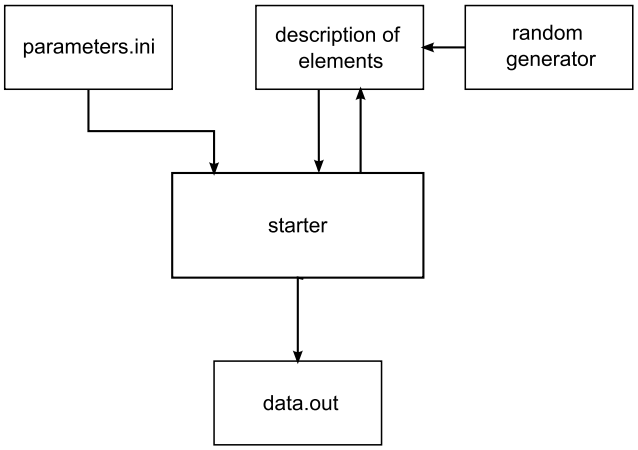

Fig. 2 Basic schema of modules of the simulation tool

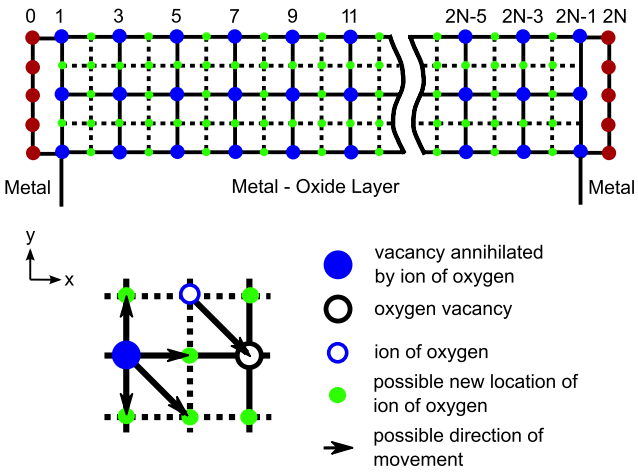

Fig. 3 A schematic picture of the unit cell of the model system

1. [Experiment]
2. type = 2
3. $n = 1$
4. [Lattice]
5. $x = 30$
6. $y = 10$
7. $z = 1$
8. def = 0
9. [RedoxEnergy]
10. E0 = 0.036
11. E1 = 5.0
12. E2 = 0.018
13. E3 = 0.036
14. E4 = 5.0
15. E5 = 0.018
16. [Stochastic]
17. $A_e = 100000$
18. $a = 2$
19. $A_i = 100$
20. $eR = 25$
21. $iR = 1$
22. [Environmental]
23. $T = 0.025$
24. [Set]
25. $U = 1.3$
26. $t = 0.0$
27. alpha = 0.1
28. beta = 0.1
29. $f = 0.5$
30. [Reset]
31. $U = -1.0$
32. $t = 0.0$
33. alpha = 0.1
34. beta = 0.1
35. $f = 0.5$
36. [Change]
37. dU = 0.01
38. dt1 = 0.01
39. dt2 = 0.001
40. dt3 = 0.01
41. dt4 = 0.00

In the module "random generator" a random number generator using the L'Ecuyer algorithm [30] was implemented. This algorithm allows random number generation with a practically infinite period (2×10^{18}).

The dimension (1D/2D/3D), size, site location, site energies, and other parameters describing the structure for the simulation are defined in the module "description of elements".

Figure 3 demonstrates an example of a unit cell for a two-dimensional array of sites. The columns with number 0 and 2N are reserved for the electrodes (anode and cathode). By moving O^{2-} from a lattice site to an interstitial a vacancy V_o

at the lattice site is formed. In the first moment of time we assume that there are no vacancies V_o in the system. Each O^{2-} has a probability Γ'_n of moving to the nearest interstitial position (if this position is empty) making a formation of a new V_o possible; moreover, each O^{2-} has a probability Γ'_n of annihilation with the nearest V_o provided this V_o is not occupied by an electron. In addition, the dynamics of electrons according to (1–3) on the vacancies V_o already formed is taken into account giving rise to the electron current in the system.

4 Model verification

All calculations were performed on one and/or two-dimensional square lattices. It was assumed that the distances between two nearest neighboring sites in all directions were equal. All V_o are at the same energy level, if no voltage is applied. Despite the fact that in the binary metal oxides, oxygen vacancies can have three different charge states with charge 0, +1, +2 [31], to simplify the calculations, we assume that the oxygen vacancy is either empty or occupied by one electron. This assumption is not a limitation, however, due to the energy separation between the three charge states, only two of them will be relevant for hopping and significantly contribute to transport.

4.1 Calculation of electron occupation probability

In order to verify the proposed model, we first evaluate the average electron occupations of hopping sites under different conditions. For comparison with previous works all calculations in this subsection are made on a one-dimensional lattice consisting of thirty equivalent, equidistantly positioned hopping sites V_o.

Following [32], we first allow hopping in one direction and only to/from the closest V_o. The occupation probability of central oxygen vacancies, p_c, is described, depending on the boundary conditions as follows: (1) for $\alpha > 0.5$ and $\beta > 0.5$, $p_c = 0.5$; (2) for $\alpha < 0.5$ and $\alpha < \beta$, $p_c = \alpha$; (3) for $\beta < 0.5$ and $\beta < \alpha$, $p_c = 1 - \beta$. Figure 4 shows simulation results of our stochastic model, which are fully consistent with theoretical predictions [32].

To move from a model system [32] to a more realistic structure, we calculated the distribution of electron occupations for a chain, where hopping is allowed not only to/from the nearest V_o (Fig. 5), and for systems, where hopping (1–3) is allowed in both directions (Fig. 6). Note that for $\alpha > 0.5$ and $\beta > 0.5$ (Figs. 5a and 6a) we still have $p_c = 0.5$ in the center, while for other values α, β we observe a decrease in p_c for $\alpha < \beta$ and an increase in p_c for $\beta < \alpha$.

We have calibrated our model in a manner to reproduce the results reported in [24], for $V = 0.6$ V to $V = 1.4$ V.

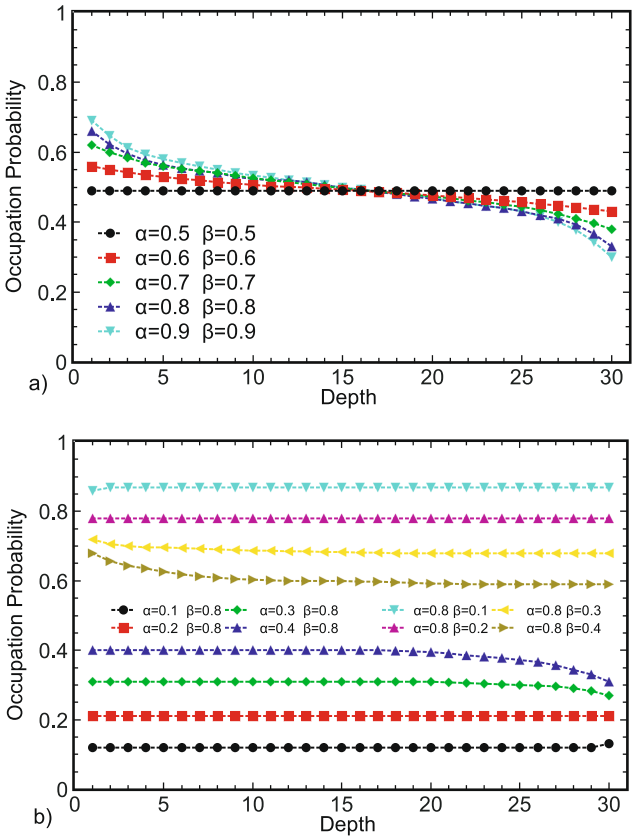

Fig. 4 Calculated distribution of electron occupation probabilities for unidirectional nearest neighbor hopping between the V_o (the 1st V_o is near the cathode, the last V_o is near the anode)

Figure 7 shows a case, where the hopping rate between two V_o is larger than the rate between the electrodes and V_o (i.e. α, $\beta < 1$). In this case a low occupation region is formed near the cathode (bipolar behavior).

Note that when $V = 0$ V, the probability of occupation of all vacancies becomes equal to 0.5 regardless of the voltage applied before. This result indicates that, after the voltage is turned off, the probability of a CF rupture should increase substantially due to a decrease of the occupation probability of the vacancies from 1 to 0.5. However, in practice we do not observe this, so to associate a CF rupture only with the formation of the low occupation region is wrong.

4.2 Modeling of the dependence of electron site occupations on temperature

With the model calibrated to [24] we simulated the temperature dependence of the site occupations in the low occupation region. The results shown in Fig. 8 demonstrate high robustness of the low occupation region demonstrating changes of less than 10%, when the temperature is elevated from 25°C to 200°C. At the same time this result indicates that the measured decrease of switching time with increasing temperature reported in [24] stems from the increased

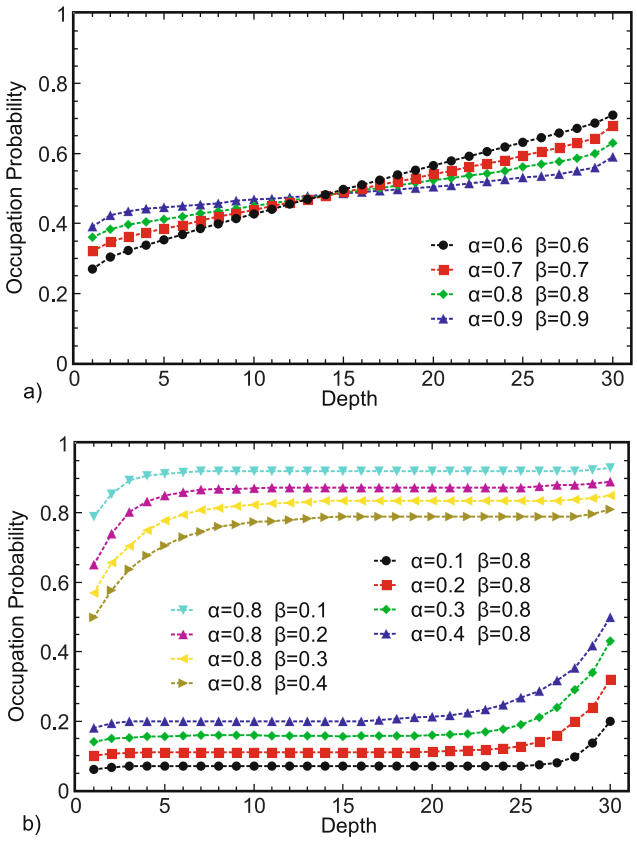

Fig. 5 Calculated distribution of electron occupation probabilities, if unidirectional hopping is allowed not only to/from the closest V_o

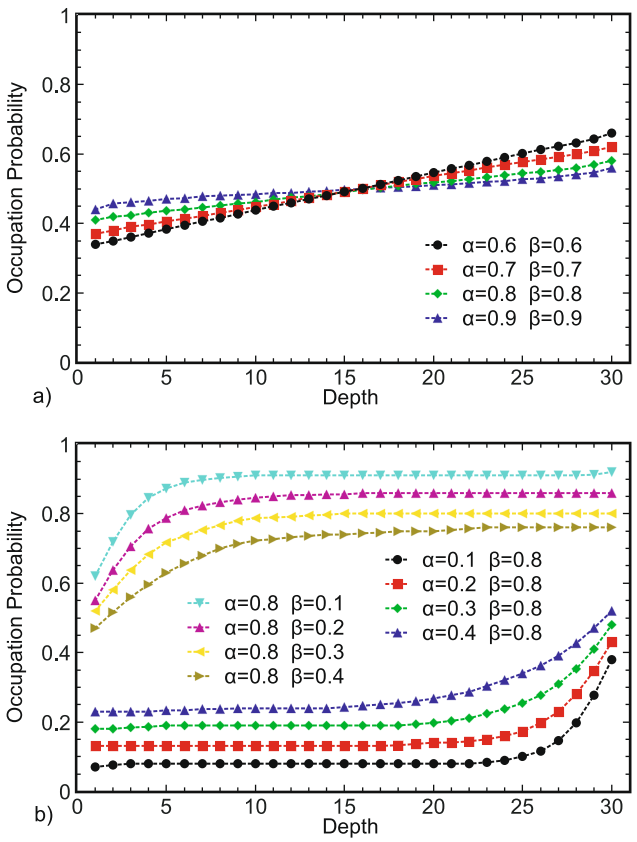

Fig. 6 Calculated distribution of electron occupation probabilities for hopping according to (1–3) for $T > 0$

mobility of oxide ions, rather than from reduced occupations of V_o in the low occupation region.

5 Results: modeling of the hysteresis cycle

All calculations of RRAM I–V characteristics are now performed on a two-dimensional lattice (10×30). We have investigated the I–V hysteresis by applying a saw-tooth like voltage V. We have assumed that the coefficients of the boundary conditions are constant and equal to 0.1. The simulated RRAM switching hysteresis cycle is shown in Fig. 9. The cycle is in good agreement with the experimental one from [8] shown in the inset of Fig. 9.

The interpretation of the RRAM hysteresis cycle obtained from the stochastic model is as follows. If a positive voltage is applied, the formation of a CF begins, when the voltage reaches a critical value sufficient to create V_o by moving O^{2-} to an interstitial position. This leads to a sharp increase in the current (Fig. 9, Segment 1) signifying a transition to a state with low resistance. When a reverse negative voltage is applied, the current increases linearly (Fig. 9, Segment 3), until the applied voltage reaches the value at which annihilation of V_o is triggered by means of moving

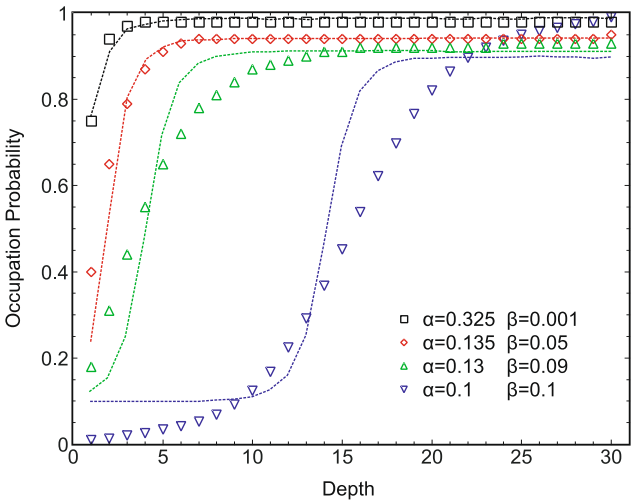

Fig. 7 Calculated distribution of electron occupation probabilities under different biasing voltages. *Lines* are from [24], *symbols* are obtained from our stochastic model

O^{2-} to V_o. The CF is ruptured and so the current decreases (Fig. 9, Segment 4). This is the transition to a state with high resistance.

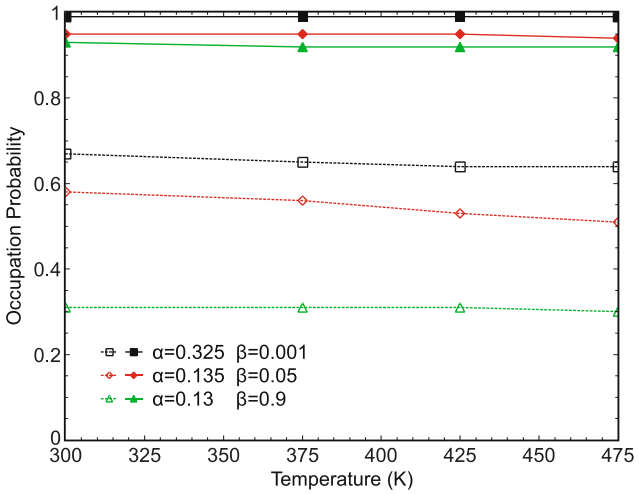

Fig. 8 Temperature dependence of electron occupation probability near the anode (*filled symbols*) and the cathode (*open symbols*)

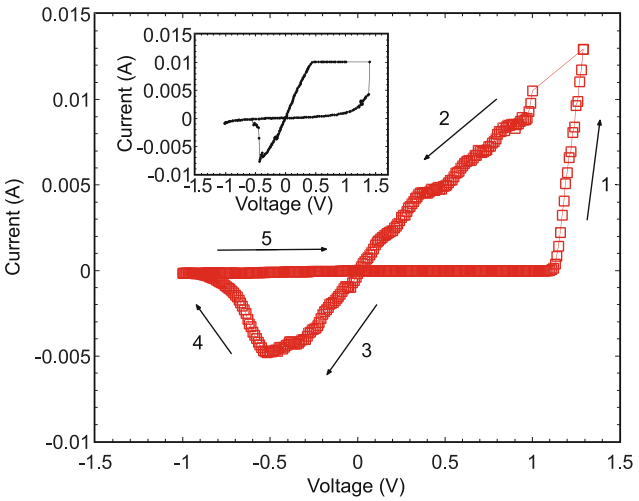

Fig. 9 I–V characteristics showing the hysteresis cycle obtained from our stochastic model ($\alpha = 0.1$ and $\beta = 0.1$). The *inset* shows the hysteresis cycle for M-ZnO-M from [8]

Figure 10 shows the hysteresis cycle obtained from the stochastic model after 5, 10, 15, and 20 cycles.

6 Conclusion

In this work we have presented a stochastic model of the bipolar resistive switching mechanism. The distribution of the electron occupation probabilities calculated with the model is in excellent agreement with previous work. The simulated RRAM switching hysteresis cycle is also in good agreement with the experimental result. We have shown that the process of rupture of the conductive filament is determined by the dynamics of oxygen ions and not only by the formation of the low occupation region. The proposed stochastic model can be used for performance optimization of RRAM devices.

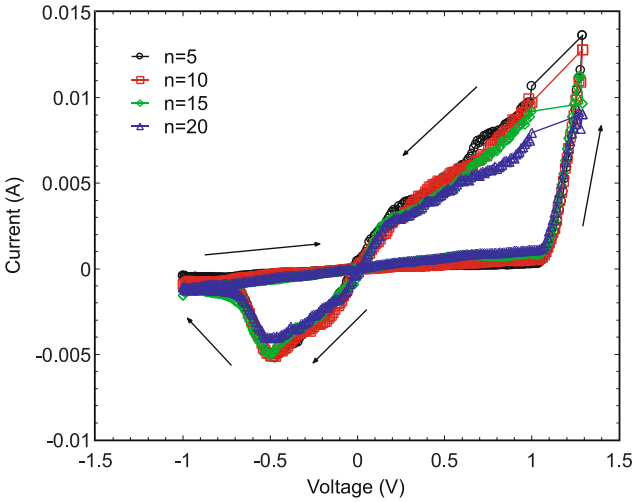

Fig. 10 Multicycle I–V characteristics showing the hysteresis cycle obtained from the stochastic model after 5, 10, 15, and 20 cycles

Acknowledgement This work has been supported by the European Research Council through the grant #247056 MOSILSPIN.

References

1. Kugeler, C., Nauenheim, C., Meier, M., Rudiger, A., Waser, R.: Fast resistance switching of TiO_2 and MSQ thin films for non-volatile memory applications (RRAM). In: NVM Tech. Symp., p. 6 (2008)
2. Yu, L.E., Kim, S., Ryu, M.K., Choi, S.Y., Choi, Y.K.: Structure effects on resistive switching of Al/TiO_x/Al devices for RRAM applications. IEEE Electron Device Lett. **29**, 331 (2008)
3. Jeong, D.S., Schroeder, H., Breuer, U., Waser R, R.: Characteristic electroforming behavior in Pt/TiO_2/Pt resistive switching cells depending on atmosphere. J. Appl. Phys. **104**, 123716 (2008)
4. Shima, H., Zhong, N., Akinaga, H.: Switchable rectifier built with Pt/TiO_x/Pt trilayer. Appl. Phys. Lett. **94**, 082905 (2009)
5. Chen, Y.S., Wu, T.Y., Tzeng, P.J.: Forming-free HfO_2 bipolar RRAM device with improved endurance and high speed operation. In: Symp. on VLSI Tech., p. 37 (2009)
6. Dong, R., Lee, D.S., Xiang, W.F., Oh, S.J., Seong, D.J., Heo, S.H.: Reproducible hysteresis and resistive switching in Metal-Cu_xO-Metal heterostructures. Appl. Phys. Lett. **90**, 42107/1-3 (2007)
7. Seo, S., Lee, M.J., Seo, D.H., Choi, S.K., Suh, D.S., Joung, Y.S., Yoo, I.K., Byun, I.S., Hwang, I.R., Kim, S.H., Park, B.H.: Conductivity switching characteristics and reset currents in NiO films. Appl. Phys. Lett. **86** (2005)
8. Lee, S., Kim, H., Yun, D.J., Rhee, S.W., Yong, K.: Resistive switching characteristics of ZnO thin film grown on stainless steel for flexible nonvolatile memory devices. Appl. Phys. Lett. **95**, 262113 (2009)
9. Watanabe, Y., Bednorz, J.G., Bietsch, A., Gerber, Ch., Widmer, D., Beck, A., Wind, S.J.: Current-driven insulator–conductor transition and nonvolatile memory in chromium-doped $SrTiO_3$ single crystals. Appl. Phys. Lett. **78**, 3738 (2001)

10. Lin, C.C., Lin, C.Y., Lin, M.H.: Voltage-polarity-independent and high-speed resistive switching properties of V-doped $SrZrO_3$ thin films. IEEE Trans. Electron Devices **54**, 3146 (2007)
11. Sawa, A., Fujii, T., Kawasaki, M., Tokura, Y.: Hysteretic current–voltage characteristics and resistance switching at a rectifying $Ti/Pr_{0.7}Ca_{0.3}MnO_3$ interface. Appl. Phys. Lett. **85**, 4073 (2004)
12. Lee, B.C., Zhou, P., Yang, J., Zhang, Y.T., Zhao, B., Ipek, E., Mutlu, O., Burger, D.: Phase-change technology and the future of main memory. IEEE MICRO **30**, 131 (2010)
13. Kryder, M.H., Kim, C.S.: After hard drives—what comes next? IEEE Trans. Magn. **45**, 3406 (2009)
14. Akarvardar, K.: Ultralow voltage crossbar nonvolatile memory based on energy-reversible NEM switches. IEEE Electron Device Lett. **30**, 626 (2009)
15. Dong, X., Wu, X., Sun, G., Xie, Y., Li, H., Chen, Y.: Circuit and microarchitecture evaluation of 3D stacking magnetic RAM (MRAM) as a universal memory replacement. In: IEEE Design Automation Conf., p. 554 (2008)
16. Bailey, R., Fox, G., Eliason, J., Depner, M., Kim, D., Jabillo, E., Groat, J., Walbert, J., Moise, T., Summerfelt, S., Udayakumar, K.R., Rodriquez, J., Remack, K., Boku, K., Gertas, J.: FRAM memory technology—advantages for low power, fast write, high endurance applications. Comput. Des., VLSI Comput. Process., 485 (2005)
17. Li, H., Xi, H., Chen, Y., Stricklin, J., Wang, X., Zhang, T.: Thermal-assisted spin transfer torque memory (STT-RAM) cell design exploration. In: Symp. on VLSI Tech., p. 217 (2009)
18. Parkin, S.P. et al., Magnetic domain-wall racetrack memory. Science **320**, 190 (2008)
19. Fujii, T., Kawasaki, M., Sawa, A., Akoh, H., Kawazoe, Y., Tokura, Y.: Hysteretic current-voltage characteristics and resistance switching at an epitaxial oxide schottky junction $SrRuO_3/SrTi_{0.99}Nb_{0.01}O_3$. Appl. Phys. Lett. **86**, 012107 (2005)
20. Nian, Y.B., Strozier, J., Wu, N.J., Chen, X., Ignatiev, A.: Evidence for an oxygen diffusion model for the electric pulse induced resistance change effect in transition-metal oxides. Phys. Rev. Lett. **98**, 146403/1-4 (2007)
21. Wu, S.X., Xu, L.M., Xing, X.J.: Reverse-bias-induced bipolar resistance switching in $Pt/TiO_2/SrTi_{0.99}Nb_{0.01}O_3/Pt$ devices. Appl. Phys. Lett. **93**, 043502/1-3 (2008)
22. Szot, K., Speier, W., Bihlmayer, G., Waser, R.: Switching the electrical resistance of individual dislocations in single-crystalline $SrTiO_3$. Nat. Mater. **5**, 312 (2006)
23. Nishi, Y., Jameson, J.R.: Recent progress in resistance change memory. In: Dev. Res. Conf., p. 271 (2008)
24. Gao, B., Sun, B., Zhang, H., Liu, L., Liu, X., Han, R., Kang, J., Yu, B.: Unified physical model of bipolar oxide-based resistive switching memory. IEEE Electron Device Lett. **30**, 1326 (2009)
25. Rozenberg, M.J., Inoue, I.H., Sanchez, M.J.: Nonvolatile memory with multilevel switching: a basic model. Phys. Rev. Lett. **92**, 178302-1 (2004)
26. Kinoshita, K., Tamura, T., Aso, H., Noshiro, H., Yoshida, C., Aoki, M., Sugiyama, Y., Tanaka, H.: New model proposed for switching mechanism of ReRAM. In: IEEE Non-Volatile Semicond. Memory Workshop, p. 84 (2006)
27. Russo, U., Ielmini, D., Cagli, C., Lacaita, A.L., Spiga, S., Wiemer, C., Perego, M., Fanciulli, M.: Conductive-filament switching analysis and self-accelerated thermal dissolution model for reset in NiO-based RRAM. In: IEDM Tech. Dig., p. 775 (2007)
28. Kim, S., Choi, Y.K.: A comprehensive study of the resistive switching mechanism in $Al/TiO_x/TiO_2/Al$-structured RRAM. IEEE Trans. Electron Devices **56**, 3049 (2009)
29. Sverdlov, V., Korotkov, A.N., Likharev, K.K.: Shot-noise suppression at two-dimensional hopping. Phys. Rev. B **63**, 081302 (2001)
30. Press, W.H., Teukolsky, S.A., Vetterling, W.T., Flannery, B.P.: Numerical Recipes in C: the Art of Scientific Computing. Cambridge University Press, Cambridge (1992)
31. Schmidt-Mende, L., MacManus-Driscoll, J.L.: ZnO-nanostructures, defects, and devices. Mater. Today **10**, 40 (2007)
32. Derrida, B.: An exactly soluble non-equilibrium system: the asymmetric simple exclusion process. Phys. Rep. **301**, 65 (1998)